Colloid Polym Sci (2002) 280:471–478
DOI 10.1007/s00396-001-0632-5

ORIGINAL CONTRIBUTION

W. Gille
B. Koschel
W. Schwieger

The morphology of isomorphous substituted hectorites

Received: 6 July 2001
Accepted after revision: 13 November 2001
Published online: 29 March 2002

W. Gille (✉) · B. Koschel
Department of Physics
Martin-Luther-University
Halle-Wittenberg
SAS-Laboratory, Hoher Weg 8
06120 Halle, Germany
E-mail: gille@physik.uni-halle.de

W. Schwieger
Lehrstuhl of Technical Chemistry I
Friedrich Alexander University
Erlangen-Nuremberg, Egerlandstrasse 3
91054 Erlangen, Germany

Abstract Small-angle scattering (SAS) is used to investigate geometric structure parameters of isomorphically substituted hectorites. The aluminum content, the layer charge, and the purity of the substituted hectorites are related to the Al supply. The structural information contained in the scattering curves $I(h)$ about the morphology of the samples in four different range orders from 1 nm to 300 nm is analyzed using the theory of the chord length distribution. The geometric structure parameters obtained are compared with results from XRD (L_0-parameter), N_2-adsorption (L_1 and mesopore size) and photon-correlation spectroscopy (largest dimension L_3 and characteristic dimension of the secondary particles).

Keywords Hectorite · Aggregation · Primary particles · Secondary particles · Range order · Stereology · Chord length distribution · Particle sizing

Introduction

Hectorite is an aluminum-free trioctahedral clay mineral with the characteristic formula $(Mg_{5.33}Li_{0.67})^{VI}(Si_8)^{IV}O_{20}(OH,F)_4Na_{0.67}{*}nH_2O$. All fundamentals including the basic structure of the silicate layers, were described between 1936 and 1958 [1, 2, 3].

The manifold application of hectorites is due to their rheological behaviour. They can be used as thickening agents with high thixotropy for aqueous and non-aqueous systems, as additives in cosmetics and pharmaceutics, and as components of domestic chemicals [4, 5, 6, 7, 8].

The smectite-type clay minerals show different properties although they differ mainly only in composition (cations at the tetrahedral and octahedral positions), but do not differ in structure. It should be possible to show the relation between the composition and the properties. We used hectorite as a model clay mineral and carried out an isomorphic substitution of silicon of the tetrahedral positions by aluminum during synthesis.

It is known from the zeolite chemistry that isomorphic substitution of silicon at tetrahedral positives by other elements, e.g. aluminum or ferrum, significantly influences the properties of the silicates (e.g. ion-exchange capacity). Such modifications possess an immense practical meaning.

Based on SAS measurements it is possible to determine size parameters and volume fractions for the special case of the hectorite particles [9]. In accordance with the parameters determined for the aluminum-free hectorite $H/0.67$-Li, a model for the hierarchical structure of these hectorite aggregates was developed, Fig. 1.

The aim of the actual investigations was the analysis of the morphology of the isomorphous substituted hectorites depending on the aluminum supply in the reaction mixture, mainly using the structural information by SAS experiments.

The methodical aspect of this article is the application of the concepts of the transformed correlation function and of the chord length distribution [10, 11, 12].

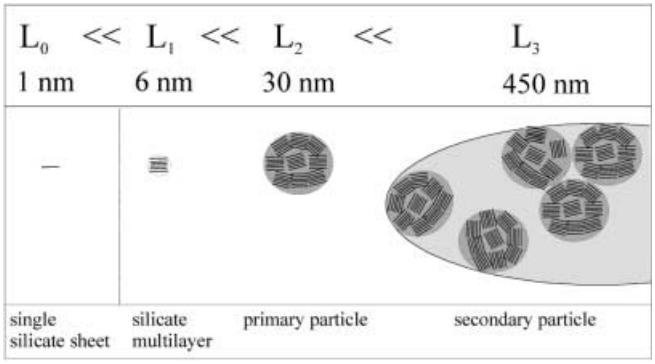

Fig. 1 Hectorite particles in four different range orders L_0, L_1, L_2, L_3

Materials and methods

Hectorite was synthesized under hydrothermal conditions at 200 °C (for details see [13]). The following molar ratios of the oxides represent the composition of the reactions:

$8SiO_2/5.33MgO/6.6Na_2O/240H_2O/0.67Li_2O/yAl_2O_3$;
$0.125 < y < 1.0$.

Silica sol, sodium hydroxide, lithium hydroxide, magnesium oxide, and sodium aluminate solutions were used as starting materials to prepare the reaction mixture. The solid content of the reaction mixture was about 20 wt-%. After a crystallization time of 24 h the product was separated by filtration, washed with deionized water and air-dried at room temperature [13]. The SAS experiments were performed by a Kratky-camera and monochromatic CuK_α radiation. The isotropic scattering curves were recorded for scattering vectors h ($h = 4\pi/\lambda \cdot \sin(\theta)$, 2θ = scattering angle), $0.015/\text{nm} < h < h_{\max} = 4/\text{nm}$. At least 5000 impulses were collected at $h = h_{\max}$, resulting from at least five cycles of the measurement. Thus, long-time intensity fluctuations, resulting from the power instability (1.5%) of the height voltage 30 KV were decreased. During the whole measurement time, the X-ray tube was running at a highly stabilized temperature of the cooling water, 23.0 °C = const., at the same laboratory temperature. This yields a sufficiently stable intensity of the trapezium profile of the primary beam, necessary for the slit length collimation correction procedure. Fundamentals of the numerical data evaluation were described in [14]. The physical principles of the data evaluation will be described in the next section.

Basic principles of data evaluation

The SAS method

SAS experiments are based on density fluctuations in the nm-region of the sample material ([10, 11, 12]). The electron density in the silicate layer (range order L_0) is defined by the more or less periodic spatial distribution of atoms of the elements Si (Si^{IV}), O, Li, Al, Mg. Density fluctuations on a larger length scale L_1 are based on the small density of the mesopores, normally filled up with air, see the model Fig. 1. The different densities of the primary and secondary particles compared with their surroundings produce fluctuations on farther reaching length scales L_2 and L_3 (see Fig. 1).

The numerical Fourier transformation of the scattering intensity $I(h)$ yields the correlation function $\gamma(r)$ (CF) [11, 12, 13]. Based on $\gamma(r)$, the so-called transformed correlation function (TCF), $\gamma_T(r)$, follows [15]. Applications of this structure function were described [16, 17, 18].

Based on $\gamma(r)$ the second derivative $\gamma''(r)$ can be obtained and interpreted on a large length scale [19, 20, 21]. The principles of this step are summarized in the next sections.

Chord length distributions (CLDs) and $\gamma''(r)$

The principles are described in the review article [19]. In the general case of an isotropic two-phase particle system of range order L, the function $\gamma''(r)$, $0 < r < L$, defines the standard scattering intensity $I(h)$ and its asymptotic expansion $I_\infty(h)$, which correspond to a certain L via:

$$I(h) = \frac{4\pi}{h^4} \cdot \int_0^L \gamma''(r) \cdot [2 - 2\cos(h \cdot r) - h \cdot r \cdot \sin(h \cdot r)]\mathrm{d}r$$

$$I_\infty(h) = \frac{-8\pi \cdot \gamma'(0)}{h^4} + \frac{16\pi \cdot \gamma'''(0)}{h^6} \qquad (1)$$

Each direct data evaluation of $I(h)$ considers the inverse relation to Eq. 1, the determination of $\gamma''(r)$ as a function of $I(h)$. By a direct way, $\gamma''(r)$ follows from $I(h)$ via Fourier transformation and numerical differentiation. Numerical differentiation procedures for experimental data demand at least one stability parameter which controls the degree of smoothness of differentiation. Here, this stability parameter is L, the upper integration limit in Eq. 1.

Numerical differentiation of $\gamma(r)$ as depending on different range orders L_i

There exist many different strategies to derive $\gamma(r)$ from $I(h)$ as well for $\gamma''(r)$ from $\gamma(r)$ (or $\gamma''(r)$ directly from $I(h)$) [12, 22]. Both differentiation steps γ-γ' and γ'-γ'' must correspond to the physical background and consequently exclusively touch a certain length interval.

The differentiation must be performed depending on a certain selected L_i. For example, the procedure for differentiating $\gamma(r)$ at $r = 3$ nm must involve the specific peculiarities of this range order and must differ from the differentiation applicable at $r = 30$ nm. For the actual problem, based on a table $\{r_k, \gamma_k(r_k)\}$, $k = 1(1)500$ with step size $\mathrm{d}r = 0.1$ nm, the second derivatives $\gamma''(r_k)$ were approximated[1] by:

$$f''(r) = f''(r,R) = \frac{\frac{f(r-R)-f(r)}{R} - \frac{f(r)-f(r+R)}{R}}{R} \qquad (2)$$

The differentiation parameter R, $R = R(L) = L/(2\pi)$, is a well-defined length. In the following, R varies in terms of the specific r-values considered between $R_0 = 1\text{ nm}/(2\pi)$ (considering small r in the range order L_0) and $R_2 = 30\text{ nm}/(2\pi)$ (considering relatively

[1] The step from the experiment to $\gamma''(r)$ requires the concentration upon a limited h-interval, $h < \pi/(1\text{ nm})$, for experiment and data evaluation. The question how exactly an experiment must be performed in order to make possible a calculation of γ'' has a simple answer, independent of the used function-system in the numerical data evaluation: $I(h)$ must be measured accurately enough so that $I'(h)$ can be calculated from the data. Then, the CLD can be determined, e.g. by use of Eq. 1 directly from a γ-table or by other procedures [14]. Worldwide, there are a lot of excellent numerical packages for data treatment and data evaluation in this field, see for example the Mathematica packages *Signals and Systems* [14].

large r in the range order L_2, see Fig. 1). The relation $R = R(r)$ used is connected with the sampling theorem of information theory. This strategy of differentiation automatically adapts the demanded "smoothness" of a differentiation result to the size of the geometric objects considered and involves a clear demarcation between different L-regions. The greater R, the stronger is the effect of smoothing. Otherwise, if no other methods of data smoothing are applied, smaller R-values (especially the limit $R \to 0$, which of course represents the exact mathematical normative) will produce an extremely structured and finely detailed second-derivative-function without any physical meaning[2]. These considerations will be applied in detail in Figs. 4, 5, 6, each of them analyzes γ'' on a different length scale.

The interpretation of the second derivative $\gamma''(r)$

Beside the CF, which is closely connected with the geometric covariance $C(r)$ ([23], page 175) and the linear erosion $P(r)$ ([24], page 323), other structure functions of stochastic geometry can be obtained from SAS experiments [23]. This includes the determination of an approximation of the CLD of the microparticle system. CLDs exclusively reflect the particle borders (the borders of the silicate phase with other regions in the hectorite sample volume).

The actual case is that of a tightly packed arrangement of particles. Dimensions from 1 nm up to 300 nm are analyzed. Two types of chord segments (denoted by l_i and m_i) exist, alternating on a test line of length 300 nm $\ll L$ through the hectorite sample.

If a straight test line intersects a two-phase system possessing a certain volume fraction c, then chord lengths l_i (within the particles) and m_i (outside the particles) result. A sequence of sum-possibilities, like $l_i + m_i$, $m_i + l_i$ or $l_i + m_i + l_i$ or $m_i + l_i + m_i$, indicates details of the particle arrangement, details of the packing-characteristics of the particles [19]. Both effects are intermixed in the function $\gamma''(r)$.

$\gamma''(r)$ reflects a sequence of chord segments

The so-called Multy Chord Distribution (MCD) is the single-particle situation of a geometric interpretation of $\gamma''(r)$ [26]. For tightly packed systems $\gamma''(r)$ reflects One Chord Distributions (OCD) as well. OCD distances are sums of chord lengths. MCD-distances always produce positive peaks in γ''. Otherwise, OCD-distances produce negative terms of γ'', if the number of chord segments in the sum of chord segments $(l_1 + m_1) + (l_2 + m_2) + \ldots$ is even. OCD-distances produce positive terms in γ'', if the number of chord segments in the sum $l_1 + m_1 + l_2 + \ldots$ is unpaired. These connections will be applied in Figs. 4, 5, 6 for the interpretation of the maximum and minimum peaks.

The distribution densities $\phi(l)$ and $f(m)$ for the isotropic case

If a system is considered in a range order L, which involves two typical (electron) densities, then here two basic CLDs exist. Let $\phi(l)$ and $f(m)$ be these CLDs. They are connected with $\gamma''(r)$.

A rod of length L possesses the CF $\gamma_{\mathrm{rod}}(r,L) = 1 - r/L$, if $r < L$ and $\gamma_{\mathrm{rod}}(r,L) = 0$, if $r > L$. Thus, γ_{rod}'' is: $\gamma_R''(r,L) = \delta(r-L)$. This function does not include any information about the distances $r < L$ at all. This is an inherent property of each CLD. Consequently, γ'' is simpler to represent and to interpret than γ. The particle border defines the particle. The inner particle parts do not influence its CLD.

General relations between $\phi(l)$, $f(m)$ and the experimental function $\gamma''(r)$

If l_i and m_i are random variables, which are independent of each other, the relation:

$$\bar{l}(1-c)\gamma''(r) = [\phi(r) + f(r) - 2\phi(r) * f(r)] * \left[\delta(r) + (\phi(r) * f(r)) + (\phi(r) * f(r))^{2*} + \ldots + \ldots\right] - 2\delta(r) \qquad (3)$$

is valid. Eq. 3 is an approximation for mutually dependent l_i, m_i. The convolution, "*", is considered in r-direction. The first moment of $\phi(l)$ is and c is the volume fraction, $\phi(r)$ and $f(r)$ define $\gamma''(r)$. It is possible to eliminate $\phi(r)$ or $f(r)$ from $\gamma''(r)$, but a complete determination without additional geometric information is not possible.

There are analytic expressions for MCDs of basic geometric figures. The mean chord length and the fourth moment of the CLD of a single convex particle are defined in terms of volume V and surface area S:

$$\bar{l} = \int_0^L l \cdot \phi(l)\mathrm{d}l = \frac{4 \cdot V}{S}, \quad \bar{l}^4 = \int_0^L l^4 \cdot \phi(l)\mathrm{d}l = \frac{12V^2}{\pi \cdot S} \qquad (4)$$

For a layer of height H, Eq. 4 yields $= 2H$. Here, H is given by the l-value of the maximum of $\phi(l)$. H equals half of the first moment of this MCD. For non-convex figures, follows from an extension of *Cauchy's* formula, Eq. 4 [19, 26].

The transformed correlation function $\gamma_{\mathrm{T}}(r)$

The following definition allows an estimation of an upper limit of the largest microparticle particle diameter via linear extrapolation [9, 15, 16],

$$\gamma_T(r) = \frac{2}{\pi} \bullet arcsin\left[1 - \gamma(r)^{\frac{1}{3}}\right], \gamma(r)0. \qquad (5)$$

Eq. 5 can be applied in cases where $\gamma(r)$ "snuggles" to the r-axis with positive values.

Results

Four samples with different Al-supplies were considered (Tables 1 and 2). The aluminum-free sample was studied in [9]. All samples have a lithium content of 0.67 mol Li_2O and differ in the Al supply in the reaction mixture. But, this parameter influences the structure, which can be detected reproducibly from the scattering behaviour.

Experimental results

The *Porod* plots were derived from the scattering intensities, see Fig. 2. In the case of a relatively small Al supply, there exist distinct *Porod* asymptotes in the recorded h-interval.

[2]This can be illustrated considering a micrograph A for a certain L_A. Each trial to recover more details in the micrograph A demands a higher magnification and consequently demands a new micrograph B which describes a smaller L_B involving finer structure elements. The micrographs A and B correspond to different R-values. It is indispensable to analyze A and B separately.

Table 1 Structure parameters of the hectorites, derived from SAS

Sample	Al supply RM[a] (mol Al_2O_3)	Layer charge (e^-/Si_4O_{10})	L_0 (nm)	L_1 (nm)	l_1[b] (nm)	L_2 (nm)	L_3 (nm)
H/0.67-Li	0	0.23	1.0	6.0	3.5	30	450
H/0.12-Al	0.125	0.27	1.2	7.5	3.5	30	210
H/0.25-Al	0.25	0.31	1.1	7.0	3.0	31	180–190
H/0.5-Al	0.5	0.40	0.85	7–10	2.5–5.5	29.5	160–170
H/1.0-Al	1.0	0.31	1.0	6–7.5	3.0	30.5	200–210

[a]Reaction mixture
[b]Mesopores between the silicate multilayers

Table 2 Structure parameters of the hectorites derived from XRD (I), N_2-adsorption (II) and photoncorrelation-spectroscopy (III)

Sample	D_{basal} (*I*) (nm)	$D_{mesopores}$ (II) (nm)	$D_{secondary\ part.}$ (III) (nm)
H/0.67-Li	1.30	2.5	400
H/0.12-Al	1.27	2.3/2.8	150
H/0.25-Al	1.27	2.3/2.8	–
H/0.5-Al	1.26	2.5	–
H/1.0-Al	1.24	2.3/2.8	200

At high Al supply both curves superimpose at large *h*-values. Here, smaller irregular inhomogeneities superimpose the characteristic *Porod* and *Kirste-Porod* behaviour of $I_\infty(h)$, Eq. 1, $h < 1$/nm. These smaller irregular microparticles with different sizes, $d < 1$ nm seems to be typical, increase $I(h)$ for larger *h*-values. In the following, these experimental results will be further analyzed, starting with larger *r*-values end ending with the 1 nm-region.

The correlation functions

The CFs in Fig. 3 allow calculation of the so-called l_p parameter[3], $-1/\gamma'(0) = l_p = \{16.8\ \text{nm},\ 12.3\ \text{nm},\ 8.7\ \text{nm},\ 11.3\ \text{nm}\}$ in the sequence of the cases from small to high Al supply. These results were obtained approximating the CFs by a linear function near the origin.

As all γ-functions are non-negative for 1 nm $< r <$ 80 nm, an estimation of the maximum extension of the primary particles L_2 (based on values 10 nm $< r <$ 20 nm) and secondary particles L_3 (based on values 40 nm $< r <$ 80 nm) was obtained via $\gamma_T(r)$.

The L_3 values for the four Al-doped samples are different (Table 1). L_3 shows smaller values for the samples with intermediate Al content.

The L_2 results can be interpreted based on Fig. 4 in the next section.

The trivial supposition, the larger the Al supply the smaller is L_3 and consequently all the other length parameters must also be smaller, is wrong. The different behaviour of the $\gamma_T(r)$ extrapolations on the upper cases in Fig. 3 does not correlate with the relatively small particles indicated by the *Porod* plots in Fig. 2. Smaller L_3-values can only lead back to a closer spatial packing of the secondary particles.

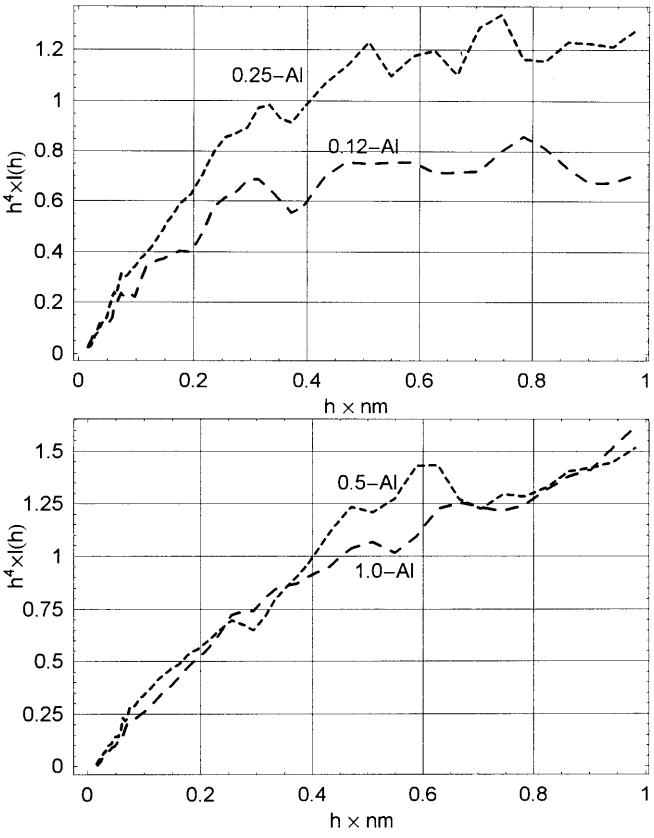

Fig. 2 Porod plots of the scattering curves, at relatively small Al supply (*above*) and relatively high Al supply (*below*)

Interpretation of $\gamma''(r)$ in terms of MCDs and OCDs

According to the theory (see above, Eq. 3), the positions of the peaks and minima of γ'' are related to each other: $\gamma''(r)$ always starts, with two well-defined positive peaks

[3]The term $-1/\gamma'(0)$ depends on *L*. More in detail, $\gamma'(0,L)$ follows from: $\gamma'(0) = \gamma'(0,L) = -\int_0^L \gamma''(r)\mathrm{d}r$

$\phi(r)$ and $f(r)$, see these terms in Eq. 3. Then, these peaks nearly define all positions of the OCDs "beforehand". From l_1 and m_1 follows l_1+m_1, $l_1+m_1+l_1$ and so on).

In cases, where $\phi(l)$ and $f(m)$ cannot be clearly detected (for example if only one first positive peak exists, because $\phi(l)$ and $f(m)$ nearly agree), the first moments can be estimated based on the OCDs. From the sum terms l_1+m_1, $l_1+m_1+l_1$ ..., l_1 and m_1 can be evaluated, too.

Considering r-values in the region L_2 and taking into account Eq. 2, $\gamma''(r)$ was plotted versus r. For 10 nm $< r <$ 30 nm, the falling curves are the upper part of the MCD $\phi_2(l)$ of the primary particles. The falling curves approximately define the dimension L_2.

For larger r-values, 40 nm $< r <$ 60 nm, the curves almost superimpose. The chord length 60 nm on this length scale nearly corresponds to the OCD value l_2+m_2. This is the average value for the distance between the centres of two primary particles. This length nearly corresponds to the minimum of $\gamma''(r)$, $\gamma''(60\text{ nm})=0$. Consequently, the volume fraction of the primary particles within a mean secondary particle can be estimated via $c_2 = 30\text{ nm}/(60\text{ nm}) = 50\%$. This estimation represents an upper limit for c_2. The ratio varies somewhat from one sample to the other. The mean value of 50% was taken into account by drawing Fig. 1. More detailed values for this volume fraction cannot be obtained from these measurements.

The measured data do not allow an exact comparison of the size distribution of the diameters d, $V(d)$, of the globular primary particles. The four curves, given in Fig. 6, are similar. Based on their arithmetic mean, it should be possible to obtain at least an approximation of $V(d)$ [26]. The result, inserted in Fig. 4, compares the mean distribution density $V(d)$ estimated with a *Rayleigh-distribution density* (RDD), with parameter $\sigma = 5.5$ nm (for more details about the background of the RDD see [27]). The deviations between the RDD and the estimation $V(d)$ are surprisingly small, which allows two conclusions:

A. The primary particles possess a spherical shape. They seem to be a relatively instable package of silicate multilayers (Fig. 1). The multilayers possess a typical diameter $L_1 = \sigma = 5$–6 nm in all considered cases (maximum position of $V(d)$).
B. The largest systematic distance between two silicate multilayers is about $L_2 = 30$ nm, (disappearing of $V(d)$ near $d = 30$ nm). More in detail, a separate calculation of $V(d)$ and inspecting exclusively the positions L_{2i} at which $V(d)$ disappears gives L_2-values $L_{21}\approx 27$ nm, $L_{22}\approx 30$ nm, $L_{23}\approx 28$ nm, $L_{24}\approx 32$ nm with increasing Al supply of the samples.

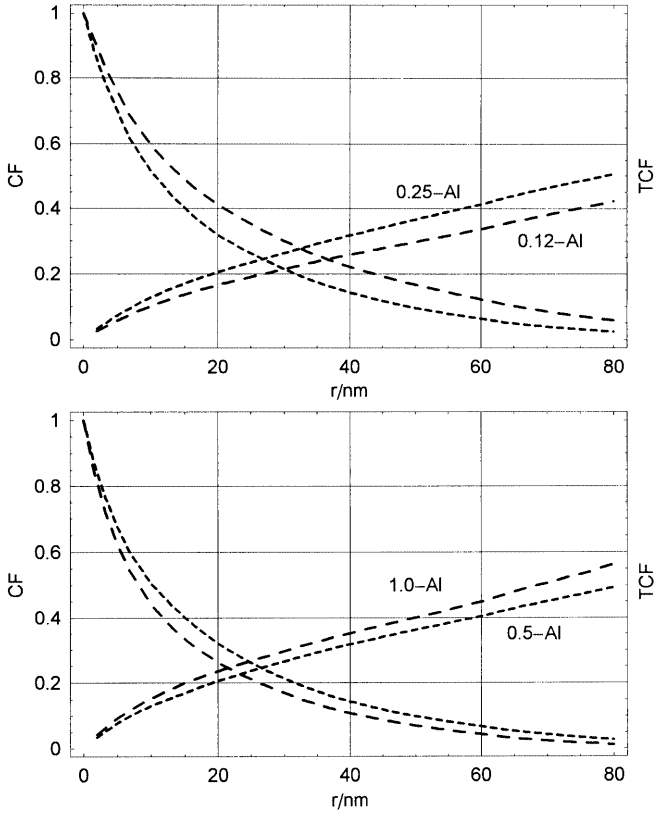

Fig. 3 Correlation functions and transformed correlation functions

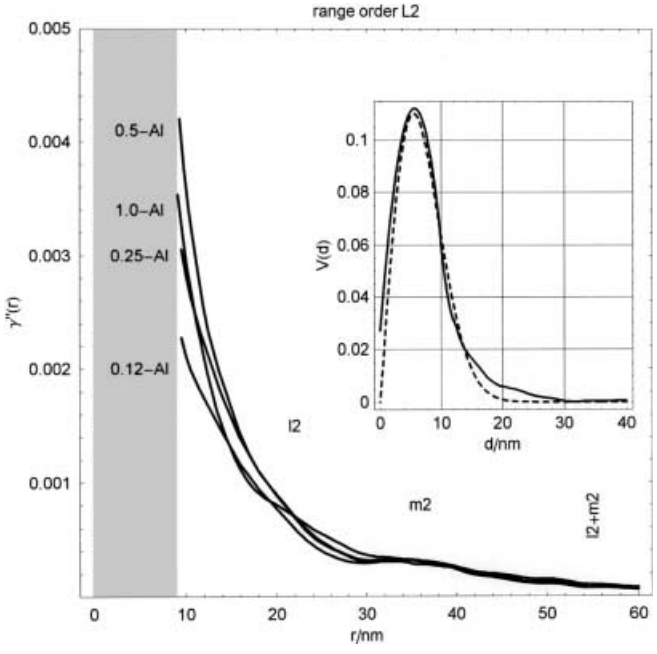

Fig. 4 The function $\gamma''(r)$ in the range order L_2, the typical diameter of the primary particles. Deviations at $r < 40$ nm can be detected. The behaviour of the four functions agrees if $r > 40$ nm. In the inset the equivalent distribution density of diameters d is compared with RDD

The second derivative of the CF is given in Fig. 5 for L_1 and Fig. 6 for L_2. The r-intervals analyzed correspond to the order ranges considered.

The interval 3 nm $< r <$ 20 nm is directly connected with L_1 (Fig. 5). As shown earlier, MCDs with mean MCD chord lengths l_1 and m_1 occur as well as OCSs. The position of some of the first OCD-convolution terms are vertically marked. Approximately, these terms can be interpreted simply as sums of the mean values of the MCDs. m_1 is interpreted to be a typical chord length of a silicate multilayer with $N = 6$ lamellas and their intermediate gaps. This mean value m_1 of 6–9 nm is the first moment of $f_1(m)$ (marked peaks in Fig. 5).

Otherwise, the mesopores are described by the MCD $\phi_1(m)$. This distribution density possesses a first moment of approximately $= l_1 = 3.5$ nm (first peaks in Fig. 5). The other peaks and the other minima represent OCDs in a nearly random sequence. These OCDs can be derived by convolution from $\phi_1(l)$ and $f_1(m)$ (Eq. 3), or approximately, by a summation of $m_1 + l_1$, $m_1 + l_1 + m_1$, and $m_1 + l_1$ plus m_1. Here, the porosity c_1 of the mesopores within a primary particle follows from $c_1 = l_1/(l_1 + m_1)$ and is about 30%–40%.

At Al supplies of 0.5-Al and 1.0-Al, the MCDs are of bimodal type (peak splitting is marked by $lm_{1A,1B}$). This behaviour differs somewhat from that one in the upper part of Fig. 5. The curve 0.5-Al reflects a more systematic arrangement, a higher degree of order than the other ones. Probably, two types of mesopores exist, with sizes down to 2.5 nm and consequently a small porosity down to 25%.

Fig. 6 allows the analysis of γ'' on a length scale up to 3 nm. Supposing a nearly symmetrical distribution of the CLDs $\phi_0(l)$ and $f_0(m)$, the single silicate layers and their gaps are detected via their mean chord length l_0 and m_0. The shoulders marked by l_0 result from the CLD of a silicate layer. Consequently, the layer heights are in the order magnitude of 0.8–1.5 nm. The positions of the mean values of the OCDs are marked vertically. These positions follow from the sums of the MCDs l_0 and m_0, the minimum position is nearly the sum $l_0 + m_0$. In these dimensions, a mean free distance (described by m_0) between the silicate layers decreases continuously depending on the Al supply.

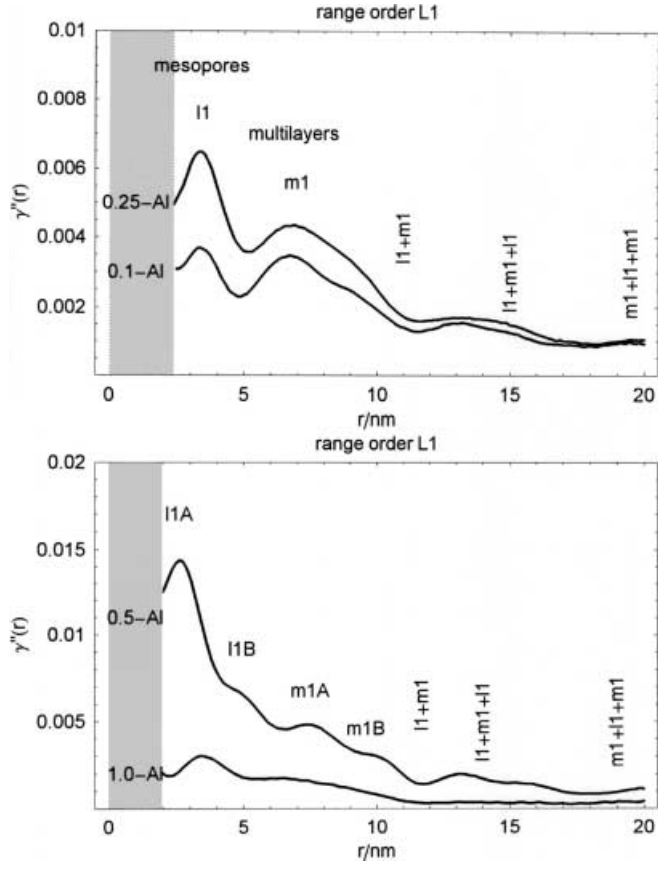

Fig. 5 The functions γ'', the sequence of the CLDs, in the range order L_1

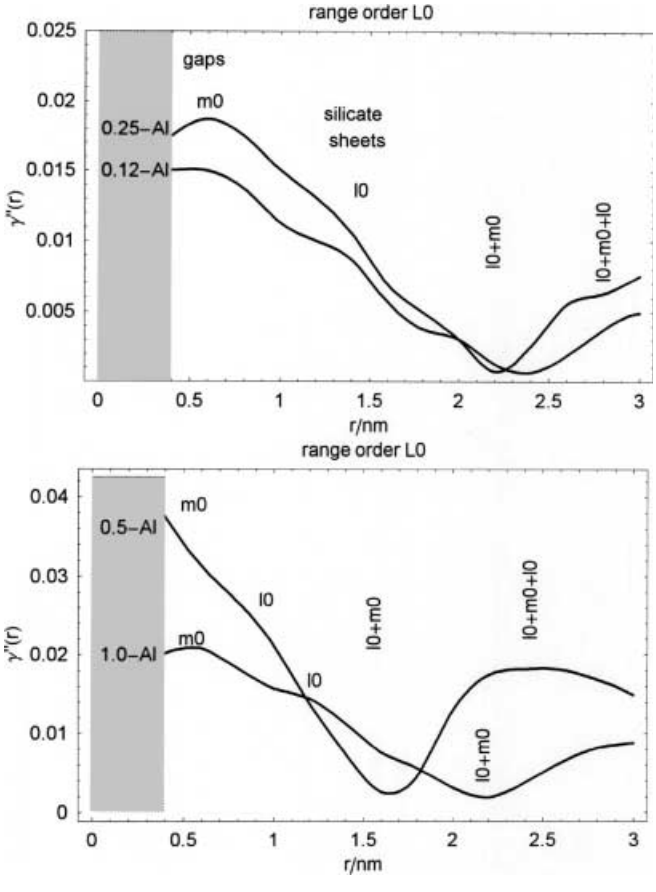

Fig. 6 The functions γ'', the sequence of the CLDs, for 0.5 nm $< r <$ 3 nm

Table 3 Structure parameters in the region L_0, derived from SAS

Samples	l_0+m_0 (nm)	m_0 (nm)	l_0 (nm)	c_0	$L_0=(l_0+m_0)/2$
H/0.12-Al	2.4	0.65	1.7	0.71	1.2
H/0.25-Al	2.2	0.60	1.6	0.73	1.1
H/0.5-Al	1.7	0.60	1.1	0.64	0.85
H/1.0-Al	2.1	0.65	1.4	0.67	1.05

With increasing Al supply, the so-called long-period of the silicate layers, $L_0=(l_0+m_0)/2$, reaches values of {(2.4/2) nm = 1.2 nm, (2.2/2) nm = 1.1 nm, (2.1/2)nm = 1.05 nm, (1.7/2) nm = 1.35 nm}. Probably, this effect can be led back to a decreasing of the intermediate spaces between the layers (see Table 3).

The volume fraction c_0 of the silica-part within a $d=5.5$ nm package follows from the MCDs l_0 and m_0 via $c_0=l_0/(m_0+l_0)$. It is $c_0=0.71$, 0.73, 0.64, 0.67 with increasing Al supply.

Discussion

The morphology does not change with the Al supply in the same way for L_0, L_1, L_2. It is necessary to distinguish between relatively small and relatively high Al contents. The results given in Figs. 2, 3, 4, 5 show the differences between these two groups.

In the first case (Al supply up to 0.25 mol Al_2O_3) the Al content of the hectorites is related to the Al supply. This is supported by the following facts:

1. The radius of Al^{3+} is smaller than that of Si^{4+}. A smaller radius of the Al^{3+} cations automatically leads to a certain "compression" of the silicate layers.
2. The amount of the negative layer charge is increased.

If the negative layer charge of a single silicate layer increases, the interaction between two neighbouring layers becomes stronger. These changes in the region of some nanometres are reflected at larger scale and the specific length parameters. Thus, the changes of the structure parameters in the sequence H/0.67-Li, H/0.12-Al, H/0.25-Al can be clearly explained. This agrees with the other data in Table 2.

If the Al supply in the reaction mixture is greater than about 0.25 mol Al_2O_3, the hectorites contain cancrinite as relatively small particles. There does not seem to exist a clear limit for this effect, but the SAS curves clearly change between H/0.12-Al and H/0.5-Al. The packing of the cancrinite particles in the hectorite samples and their electron density distribution yield a superposition of the scattering curves (Figs. 3 and 4). This agrees with the structure parameters of the H/0.5-Al sample (line 4 in Table 1): The highest negative layer charge corresponds to the smallest values of L_3, L_2, L_1, and L_0. The layer charges of the other three Al-containing hectorite samples are similar, about $0.3e^-/Si_4O_{10}$. It is remarkable that the estimated L_3-values of those samples are also similar (about 200 nm).

Summary

The substitution of Si^{4+} by Al^{3+} is not linearly related to the Al supply. The influence on the morphology is summarized in Tables 1, 2, 3. The following geometric parameters were estimated:

(a) The long period L_0 of the silicate layer is 0.8–1.2 nm; (b) the silicate lamellae consist of a maximum of six silicate layers, because the maximum dimension of the multilayers is about 7 nm; for the primary particles a maximum dimension of 29–31 nm was determined; the maximum dimension of the secondary particles was estimated of about 210 nm; the differences already recognizable in the SAS curves are more clearly expressed by the structure functions γ, γ'', $\gamma_T(r)$.

The formal determination of the equivalent diameter-distribution up to $d=40$ nm yields a distribution density $V(d)$ which can be approximated by a *Rayleigh-distribution density* with a length parameter $\sigma=5.5$ nm. In this light, $V(d)$ seems to describe the nearly spherical primary particles as well as the silicate multilayers (insert in Fig. 4). From Figs. 3, 4, 5, 6, it follows that approximately 20 primary particles and the corresponding intermediate volumes form one typical secondary particle with maximum diameter L_3.

In cases of a small Al supply, the mesopores are nearly regularly arranged in space and possess a relatively narrow size distribution, $3\text{ nm} < l < 3.5$ nm,

On the other hand, the geometric arrangement is less regular for Al supplies higher than 0.5 mol Al_2O_3. Here, complicated bimodal distributions seem to exist.

References

1. Foshag WF, Woodford AO (1936) Am Miner 21:238
2. Strese H, Hofmann U. (1941) Z Anog allg Chem 247:65
3. Ames LL, Sand LB, Goldich SS (1958) Econ Geol 53:22
4. Van Oss, CJ, Giese RF, Costanzo PM (1990) Clays and Clay Minerals 38:151
5. Bachmann V (1988) J Coll and Interface Sci 126:1
6. Riegelmann MA (1963) Farbe u Lack 69:684
7. Neumann T (1968) J Oil Coll Chem Assoz 51:232
8. Yamaguchi T (1990) J SCCJ 24:119
9. Koschel B, Gille W, Schwieger W, Janowski F (2000) Coll Polym Sci 278:805
10. Porod G (1951, 1952) Koll Zeitschrift 124:83, 125:51
11. Debye P Bueche AM (1949) J Appl Phys 20:518
12. Feigin LA, Svergun DI (1987) Structure analysis by small-angle x-ray and neutron scattering, Plenum, New York
13. Koschel B (2000) Struktur-Eigenschafts-Beziehungen isomorph substituierter Hectorite, Wissenschaft, Reihe Chemie, Bd 291, Tectum, Marburg
14. Gille W (1994) J Physique IV/I, 3-C8:503
15. Gille W (2000) Comp Mater Sci 18:65
16. Gille W, Enke D, Janowski F (2001) J Porous Mater 8:111
17. Enke D, Janowski F, Gille W, Schwieger W (2001) Coll and Surf A: Physicochem Eng Aspects 187:131
18. Enke D, Otto K, Janowski F, Schwieger W, Gille W (2001) J Mater Sci 36:2349
19. Gille W (2000) The Europ Phys J 17:371
20. Cabo AJ, Baddeley AJ (1995) Adv Appl Prob 27:585
21. Lu B, Torquato S (1993) J Chem Phys 98:6472
22. Wolfram Research, Inc (1999) Mathematica, version 3, Champaign, Illinois
23. Stoyan D, Kendall WS, Mecke J (1987) Stochastic geometry and its applications, Akademie Verlag, Berlin
24. Serra J (1982) Image analysis and mathematical morphology, Academic Press, London
25. Stribeck N, Ruland W (1978) J Appl Cryst 11:535
26. Damaschun G, Pürschel HV (1969) Monatshefte Chemie 100:247
27. Gille W (1999) Nano Structured Mater 11:1269
28. Gille W (1995) Das Konzept der Sehnenverteilung zum Informationsgewinn aus einer Kleinwinkelstreukurve und seine Grenzen, Habilitation, Halle